Highly Conjugated *p*-Quinonoid π-Extended Tetrathiafulvalene Derivatives: A Class of Highly Distorted Electron Donors

Marta C. Díaz,[a] Beatriz M. Illescas,[a] Nazario Martín,*[a] Rafael Viruela,[b] Pedro M. Viruela,[b] Enrique Ortí,*[b] Ortwin Brede,*[c] Israel Zilbermann,[d, e] and Dirk M. Guldi*[d]

Dedicated to Professor Jose L. Soto on the occasion of his retirement

Abstract: A new class of π-extended TTF-type electron donors (**11a–c**) has been synthesized by Wittig–Horner olefination of bianthrone (**9**) with 1,3-dithiole phosphonate esters (**10a–c**). In cyclic voltammetry experiments, donors **11a–c** reveal a single, electrochemically irreversible oxidation—yielding the corresponding dicationic products—at relatively low oxidation potentials (~0.7–0.8 V). Theoretical calculations, performed at the DFT level (B3P86/6-31G*), predict a highly-folded C_{2h} structure for **11a**. In the ground state, the molecule adopts a double saddle-like conformation to compensate the steric hindrance. The calculations suggest that the intramolecular charge transfer associated with the HOMO→LUMO transition is responsible for an absorption band observed above 400 nm. While the radical cation **11a**$^{\cdot+}$ retains the folded C_{2h} structure predicted for the neutral molecule as the most stable conformation, the dication **11a**$^{2+}$ has a fully aromatic D_2 structure, formed by an orthogonal 9,9′-bianthryl central unit to which two singly-charged dithiole rings are attached. The drastic conformational changes that compounds **11** undergo upon oxidation account for their electrochemical properties. By means of pulse radiolysis measurements, radical-induced one-electron oxidation of **11a–c** was shown to lead to the radical cation species (**11a–c**$^{\cdot+}$), which were found to disproportionate with generation of the respective dication species (**11a–c**$^{2+}$) and the neutral molecules (**11a–c**).

Keywords: cyclic voltammetry · density functional calculations · pulse radiolysis · sulfur heterocycles · tetrathiafulvalene

Introduction

Over the past three decades, much attention has been focused on the development of new planar electron donors as integrative building blocks for organic conductors. In this context, the use of π-conjugated planar electron donors and acceptors has been recognized as a successful approach to the assembly of electrically conducting molecular crystals, in which donors and acceptors form segregated stacks.[1] Tetrathiafulvalenes (TTF, **1**) and their derivatives, including those that incorporate other chalcogenides (i.e., Se and Te), emerged as nearly planar electron-donor molecules and have been extensively used in the preparation of electrically conducting and superconducting molecular materials.[2]

Particularly interesting electron donors are 9,10-bis(1,3-dithiol-2-ylidine)-9,10-dihydroanthracene derivatives (exTTF, **2**). Despite their highly distorted structures, which show a discernible deviation from planarity,[3] electrically conducting charge-transfer complexes (CTC) have been prepared by reacting these donors with strong electron acceptors such as tetracyano-*p*-quinodimethane (TCNQ).[4] Recently, these

[a] M. C. Díaz, Dr. B. M. Illescas, Prof. Dr. N. Martín
Departamento Química Orgánica
Facultad de Ciencias Químicas, Universidad Complutense
28040 Madrid (Spain)
E-mail: nazmar@quim.ucm.es

[b] Prof. Dr. R. Viruela, Prof. Dr. P. M. Viruela, Prof. Dr. E. Ortí
Departamento Química Física
Instituto de Ciencia Molecular
Universitat de València
46100 Burjassot (Spain)
E-mail: enrique.orti@uv.es

[c] Prof. Dr. O. Brede
Universität Leipzig
Interdisziplinäre Arbeitsgruppe "Zeitaufgelöste Spektroskopie"
04303 Leipzig (Germany)

[d] Dr. I. Zilbermann, Prof. Dr. D. M. Guldi
Radiation Laboratory, University of Notre Dame
Indiana, IN 46556 (USA)
E-mail: guldi.1@nd.edu

[e] Dr. I. Zilbermann
On sabbatical leave from Nuclear Research Centre Negev
Beer Sheva (Israel)

 DOI: 10.1002/chem.200305555

p-quinonoid π-extended TTF derivatives (exTTF), which release two electrons simultaneously in a single quasi-reversible electron-transfer process, have been covalently linked to various electron-acceptor molecules, affording topologically diverse donor–acceptor (D–A) systems. Several interesting physico-chemical properties have been reported for these D–A systems, such as: i) nonlinear optical effects with **3**,[5] ii) efficient monitoring of metal complexation when, for example, a crown-ether moiety is fused to exTTF **4**,[6] and iii) isolation of covalent D^{2+}-σ-$A^{\bullet-}$ species.[7]

The interest in implementing exTTFs in fields other than organic conductors led to a need for the development of synthetic methodologies that would allow access to functionalized exTTF derivatives that could serve as versatile building blocks in the design of more sophisticated architectures.[8]

During recent years, we have directed our efforts towards covalently linking exTTF systems to electron acceptors such as C_{60}.[9,10] The remarkable electron-acceptor properties of fullerenes, that is, their ability to accept up to six electrons in solution,[11] prompted us to try to integrate them into novel artificial photosynthetic systems.[12] Our approach to the design of C_{60}-based D–A systems is based on molecular donor units that become aromatic upon oxidation. In fact, the gain of aromaticity is central to the stabilization of the charge-separated state.[13] TTF and, particularly, exTTF fulfil these requirements and to demonstrate the benefits of this aromaticity concept we report here on the dyads **5**–**7**, for which charge-separated state lifetimes ranging from a few nanoseconds (**5**) to several hundreds of nanoseconds (**6**, **7**) have been measured.[9] Moreover, the use of gradient redox centers, by linking, for example, two different exTTF units to C_{60} (**8**) extends the charge-separated state lifetime to a value of the order of ~100 μs.[10c] The long lifetimes in exTTF/C_{60} dyads can be rationalized on the basis of the low reorganization energy of C_{60}[14] coupled with the gain of aromaticity/planarity of the exTTF moieties which occurs upon oxidation.[3]

Our interest in developing novel π-extended TTF architectures that would show an even more pronounced gain of aromaticity and planarity during their oxidation processes initiated a pursuit of bianthracene electron-donor derivatives (**11a–c**). Bianthracene compounds are composed of two independent anthracene skeletons, in which the two dithiole rings are separated by much greater distances than, for example, in exTTFs (**2**). Consequently, it seems reasonable to expect an even greater gain of aromaticity and increase in planarity during the oxidation process.

We report herein on the synthesis of a new class of bianthracene electron donors (**11a–c**) and the spectroscopic characterization of their oxidized species by means of radiation chemical and electrochemical techniques. The present work is complemented by theoretical calculations at the density functional theory (DFT) level in order to shed light on the structural and electronic properties of these electron-donor molecules.

Abstract in Spanish: *Una nueva familia de moléculas dadoras de electrones de tipo TTF π-extendido, altamente conjugadas, (**11a–c**) se han sintetizado mediante la reacción de olefinación de Wittig–Horner de la biantrona (**9**) con fosfonatos de 1,3-ditiol (**10a–c**). En los experimentos de voltamperometría cíclica, los dadores **11a–c** muestran una única onda de oxidación electroquímicamente irreversible—dando lugar a los productos dicatiónicos—a potenciales relativamente bajos (~0.7–0.8 V). Cálculos teóricos, llevados a cabo a nivel DFT (B3P86/6-31G*), predicen una estructura C_{2h} altamente distorsionada para **11a**. La molécula adopta una conformación en forma de doble mariposa para aliviar el impedimento estérico. Los cálculos sugieren que la transferencia de carga intramolecular asociada a la transición HOMO→LUMO es responsable de la banda de absorción observada por encima de 400 nm en el espectro electrónico. El catión radical **11a**$^{\bullet+}$ retiene la estructura C_{2h} plegada predicha para la molécula neutra como la conformación más estable. Por el contrario, el dicatión **11a**$^{2+}$ muestra una estructura D_2 totalmente aromática, formada por una unidad central de 9,9′-biantrilo ortogonal, unida a los anillos cargados de ditiol. Los profundos cambios conformacionales que experimentan los compuestos **11** tras la oxidación explican sus propiedades electroquímicas. Medidas de radiólisis de pulso, esto es, la oxidación monoelectrónica de **11a–c** inducida por radicales, conduce a las especies catión radical (**11a–c**$^{\bullet+}$), las cuales dismutan para generar las respectivas especies dicatiónicas (**11a–c**$^{2+}$) y la molécula neutra (**11a–c**).*

Results and Discussion

Synthesis: The novel electron-donor molecules **11a–c** were prepared according to the protocol summarized in Scheme 1. The Wittig–Horner olefination reaction of commercially available and poorly soluble bianthrone (**9**) with the carbanion of phosphonate esters **10a–c**, generated in the presence of *n*-butyllithium at −78 °C, afforded bis(1,3-dithiol-2-ylidene)-9,9′-bis(9,10-dihydroanthracene) derivatives **11a–c** as air-stable orange solids in good yields.[15] The precursors, that is, phosphonate esters (**10a–c**), were prepared by way of a multi-step synthesis starting from substituted 1,3-dithiole-2-thiones.[16]

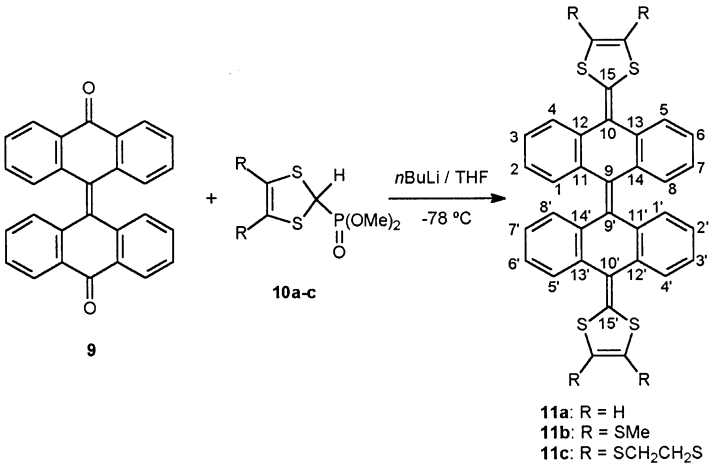

Scheme 1.

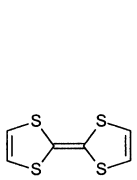

TTF, **1**

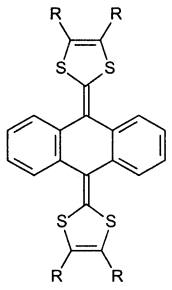

exTTF, **2**
R = H, SCH_3, $(SCH_2)_2$

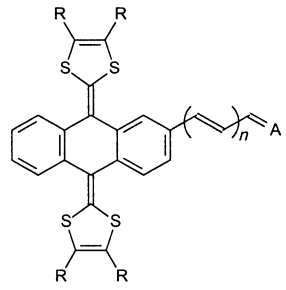

3 : R = H, SCH_3, $(SCH_2)_2$
A = $C(CN)_2$; *p*-NO_2-C_6H_4-
n = 0, 1, 2

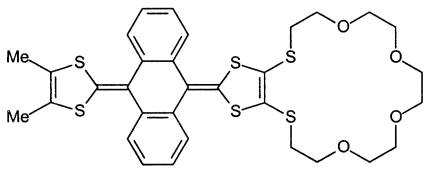

4: R = H, SCH_3, $(SCH_2)_2$

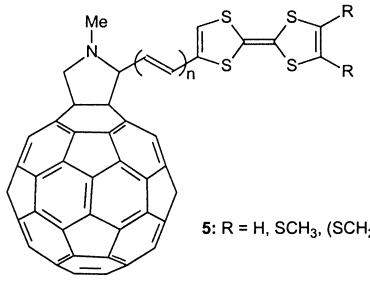

5: R = H, SCH_3, $(SCH_2)_2$

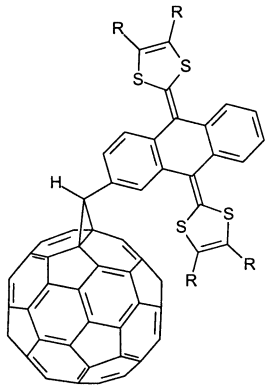

6: R = H, SCH_3, $(SCH_2)_2$

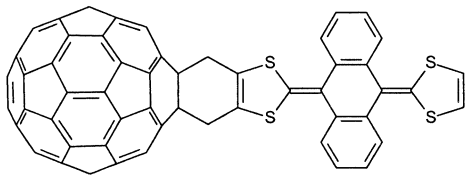

7: R = H, SCH_3, $(SCH_2)_2$

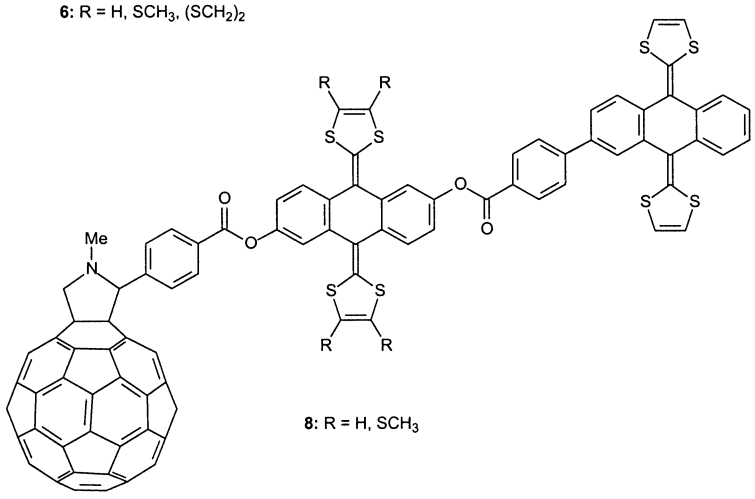

8: R = H, SCH_3

dithiole rings as a singlet at δ = 6.34 (4H) for **11a**, a singlet at δ = 2.50 ($4SCH_3$) for **11b**, and a multiplet at δ = 3.37 ($4\text{-}CH_2\text{–}S$) for **11c**. The structures of compounds **11a–c** were further verified by mass spectrometry.

Figure 1 shows the UV/Vis spectrum recorded for **11a** in dichloromethane solution; the spectra of **11b** and **11c** exhibit similar optical absorption features. All three compounds have a broad absorption band above 400 nm. In **11a**, the band appears at 431 nm and shifts bathochromically for **11b** (436 nm) and **11c** (450 nm) due to the electron-releasing character of the substituents attached to the dithiole rings (i.e., SCH_3 and $(SCH_2)_2$). It should be noted that the λ_{max} values measured for compounds **11a–c** are similar to those previously reported for the related compounds **2a–c** (**2a**: 428 nm; **2b**: 434 nm; **2c**: 446 nm).[17] The shifts are small in spite of the larger size of the conjugated bianthracene spacer in **11a–c**, which suggests that the electronic interaction between the two anthracene units is rather weak. The UV/Vis data are discussed further in the theoretical section.

Electrochemistry: The redox potentials of **11a–c** were determined by cyclic voltammetry (CV) measurements, carried out at a scan rate of 100 $mV\,s^{-1}$ in dichloromethane solution at room temperature with tetrabutylammonium perchlorate (0.1 M) as supporting electrolyte, Ag/Ag^+ as a reference electrode, and GCE as the working electrode. Figure 2 depicts the CV recorded for **11a** as a representative example.

Compounds **11a–c** showed low solubility in common organic solvents and, therefore, we were unable to record their ^{13}C NMR spectra. Despite this, the spectroscopic data support the proposed structures. The ^1H NMR spectra of **11a–c** show, in addition to the expected signals of the anthracene moieties, signals due to the substituents on the 1,3-

Compounds **11a–c** give rise to an electrochemically irreversible oxidation wave, involving two electrons, during which the respective dications are formed (**11a**: $E_{ap}^{1,ox}$ = 0.74 V; **11b**: $E_{ap}^{1,ox}$ = 0.81 V; **11c**: $E_{ap}^{1,ox}$ = 0.82 V). The reduction wave, corresponding to the reversion of the dication to the neutral molecule, is observed at negative values (**11a**:

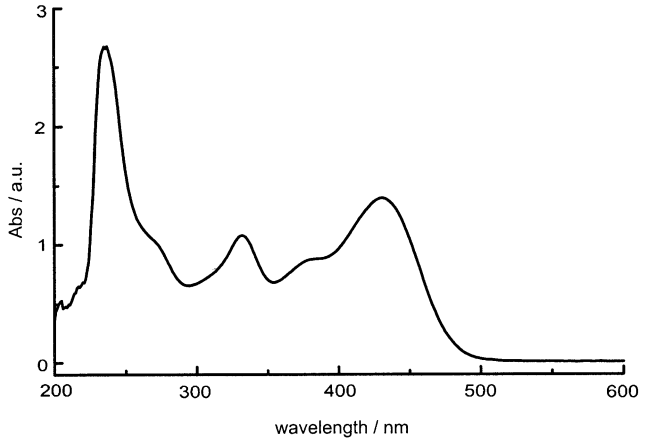

Figure 1. UV/Vis absorption spectrum of compound **11a** in dichloromethane at room temperature.

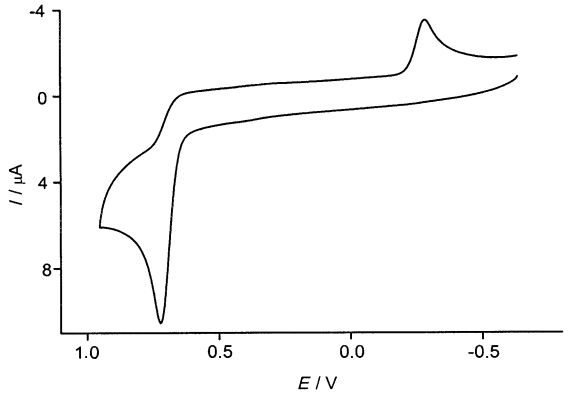

Figure 2. Room temperature cyclic voltammogram of **11a** in dichloromethane (scan rate: 100 $mV\,s^{-1}$; working electrode: glassy carbon; reference electrode: Ag/Ag^+; supporting electrolyte: Bu_4NClO_4).

$E_{cp}^{1,red} = -0.25$ V; **11b**: $E_{cp}^{1,red} = -0.11$ V; **11c**: $E_{cp}^{1,red} = -0.09$ V). The large splitting between the oxidation and the reduction potentials could suggest, among other possibilities, a high activation barrier when going from the dication state to the neutral molecule. As is generally observed for TTF derivatives, the unsubstituted compound **11a** shows a better donor character than **11b,c**, despite the electron-releasing character of the SCH_3 and $(SCH_2)_2$ substituents. This effect has been discussed in relation to the parent TTF molecule, and can be attributed to solvation interactions that lead to a greater stabilization of the oxidized species in the case of the unsubstituted dithiole rings.[18]

The electrochemical behavior of the novel donors **11a–c** is similar to that observed for the related structures **2a–c**.[3,4] In the latter case, the two-electron nature of the oxidation wave is well established,[15] the coalescence being attributable to the structural rearrangement that accompanies the redox process, namely the transformation of a strongly bent neutral state into a fully aromatic dication species.[3,4a,8d,19] A similar structural rearrangement can be expected for **11a–c**. As previously shown for compounds **2**,[15,19,20] the scan rate and the temperature at which the CV measurements are made are of critical importance with regard to the electrochemical behavior. These factors strongly influence the equilibrium between the species appearing during the oxidation/reduction processes, and can be correlated with the conformational rearrangements that accompany these processes.

Electrochemical data for **11a** have been previously reported by Bryce et al.[15] Interestingly, compounds **11a–c** exhibit an inferior electron-donor ability in comparison with exTTF ($E_{ap}^{1,ox} = 0.40$ V).[20] The shift in oxidation potential can be rationalized in terms of the large distance separating the two dithiole rings, which in **11a–c** behave as nearly independent units connected through a hydrocarbon skeleton.[21]

Theoretical calculations: To gain a deeper understanding of the experimental trends, the molecular structures and electronic properties of the neutral and oxidized states of **2a** and **11a** were theoretically investigated. Here, **2a** was studied as a reference system. Most of the calculations were performed within the density functional theory (DFT) approach using the gradient-corrected B3P86 hybrid functional and the 6-31G* basis set (B3P86/6-31G*). DFT calculations include electron correlation effects at a relatively low computational cost and are known to provide accurate equilibrium geometries.[22]

Neutral compounds: As discussed in a preceding paper,[3] the minimum-energy conformation of **2a** corresponds to a butterfly-shaped nonplanar C_{2v} structure. The structure is illustrated in Figure 3a. The planar D_{2h} structure of the molecule is strongly hindered by the very short contacts (1.978 Å) between the sulfur atoms and the hydrogen atoms in the *peri* positions. To relieve these interactions, the central ring folds into a boat conformation and the molecule adopts a butterfly- or saddle-like structure, in which the benzene rings point upwards and the dithiole rings point downwards. The resulting C_{2v} conformation is more stable than the fully planar D_{2h} structure by 37.71 $kcal\,mol^{-1}$, and is perfectly consistent with the crystal structures observed for different derivatives of **2**.[4a,8d,19]

In compounds **11a–c**, additional steric repulsion arises between the hydrogen atoms at the 1,8′ and 1′,8 *peri* positions in the inter-anthracene region (see Scheme 1 for atom numbering). To relieve these interactions, the molecule of **11a** folds, in a similar manner as a molecule of **2a**, so as to adopt a double-butterfly or saddle-like structure in which the two anthracene moieties are bent away from one another (see Figure 3b). The minimum-energy structure predicted theoretically has a center of symmetry (i.e., C_{2h} point group) and is consistent with the X-ray crystal structures reported for the bianthrone molecule[23] and for an electron-acceptor analogue of **11a** in which the dithiole rings are replaced by dicyanomethylene units.[24]

The distortions from planarity of molecule **11a** can also be described in terms of various angles. Thus, the anthracene systems are folded along the C9···C10 and C9′···C10′ vectors by 42.3°. This value compares well with that reported for the bis(dicyanomethylene) analogue of **11a**[24] and those found for a series of derivatives of **2a** (35–45°).[4a,8d,19] The outer benzene rings preserve their planarity and are rotated by an average angle of 44.1° out of the plane of the

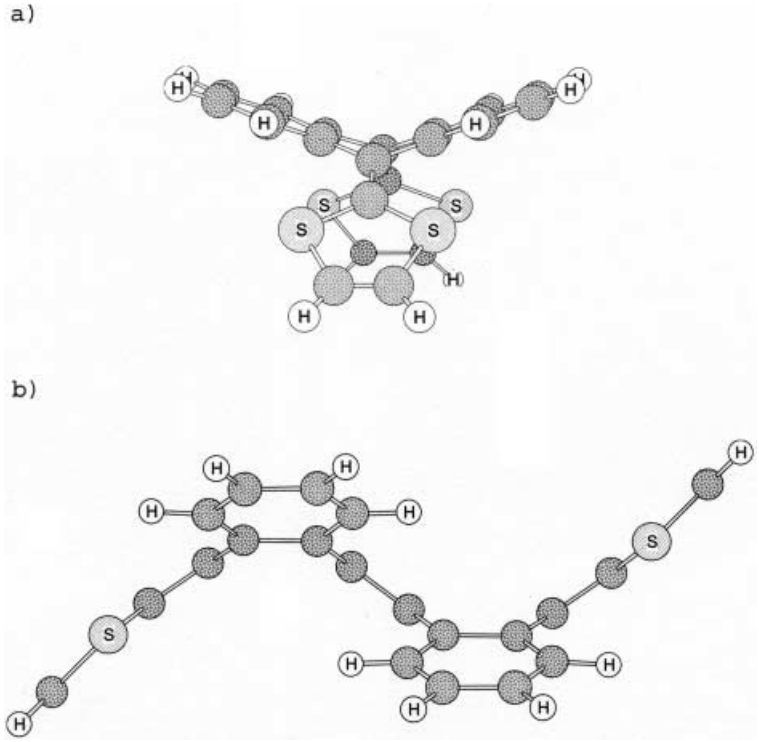

Figure 3. Minimum-energy B3P86/6-31G*-optimized conformations: a) compound **2a** (C_{2v} symmetry); b) compound **11a** (C_{2h} symmetry).

central ethylene subunit. The dithiole rings are each tilted by 34.5° with respect to the planes defined by atoms C11-C12-C13-C14 and C11′-C12′-C13′-C14′, respectively. Overall, the rings are folded by 8.0° along their S···S axes.

Figure 4a summarizes the B3P86/6-31G*-optimized values for selected bond lengths of **11a**. Apart from the carbon–carbon (CC) bonds of the dithiole rings (1.336 Å), the shortest bond lengths correspond to the exocyclic C9–C9′, C10–C15, and C10′–C15′ bonds (~1.36 Å) that link the four structural subunits. The outer benzene rings of the anthracene units preserve their aromaticity, since all the CC bonds forming these rings have a length of 1.40 ± 0.01 Å and define internal bond angles of $120 \pm 1°$. The CC bonds that connect the benzene rings with the exocyclic C=C bonds, on the other hand, have mainly single-bond character (~1.48 Å). In summary, the molecular structure of **11a** can be visualized as three ethylene groups linked together by four aromatic benzenes and end-capped with two electron-donor dithiole rings.

In Figure 5 the atomic orbital (AO) compositions calculated for the highest occupied molecular orbital (HOMO) and the lowest unoccupied molecular orbital (LUMO) of **11a** are displayed. While the HOMO is mainly localized on the dithiole rings, with significant contributions from the exocyclic C=C bonds, the LUMO extends over the anthracene units with small contributions from the dithiole rings. Compared with **2a**, for which the HOMO presents a similar AO composition and is calculated to lie at −5.23 eV, the HOMO of **11a** lies at −5.35 eV. This stabilization justifies, to a first approximation, the more positive oxidation potential recorded for **11a**.

To investigate the nature of the electronic transitions that give rise to the absorption bands observed in the experimental UV/Vis spectrum, the electronic excited states of **11a** were calculated using the time-dependent DFT (TDDFT) approach and the B3P86/6-31G*-optimized geometry. Our calculations predict that the lowest-energy absorption band observed at 431 nm (2.87 eV) for **11a** is due to excitation to the first electronic excited state (1^1B_u), which is calculated to lie 2.70 eV above the ground state (1^1A_g). For this $1^1A_g \rightarrow 1^1B_u$ electronic transition we calculated an oscillator strength (*f*) of 0.39. This transition corresponds mainly to the promotion of one electron from the HOMO to the LUMO. As shown in Figure 5, the HOMO→LUMO promotion implies some electron-density transfer from the dithiole rings, on which the HOMO is mainly located, to the anthracene units. Calculations therefore suggest that the first absorption band observed at 431 nm implies some intramolecular

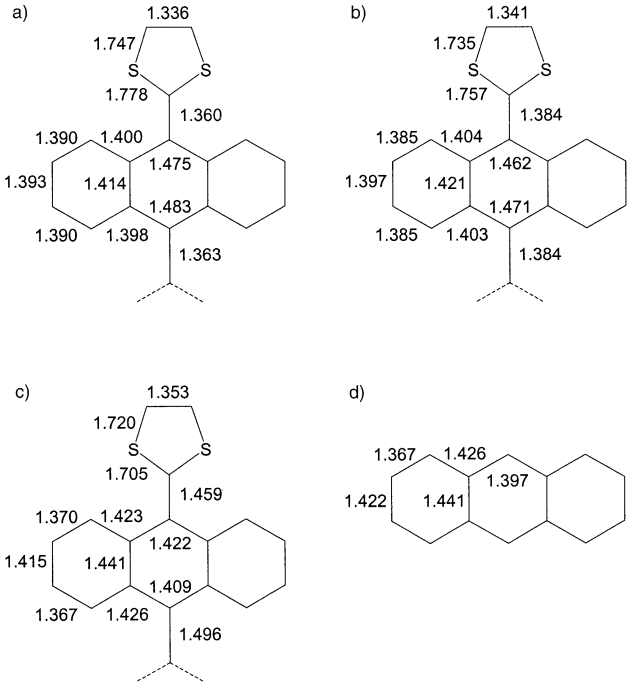

Figure 4. B3P86/6-31G*-optimized bond lengths [Å] calculated for a) neutral **11a** (C_{2h} symmetry), b) **11a**$^{\cdot+}$ (C_{2h} symmetry), c) **11a**$^{2+}$ (D_2 symmetry), and d) anthracene (D_{2h} symmetry). Only a half of molecule **11a** is depicted.

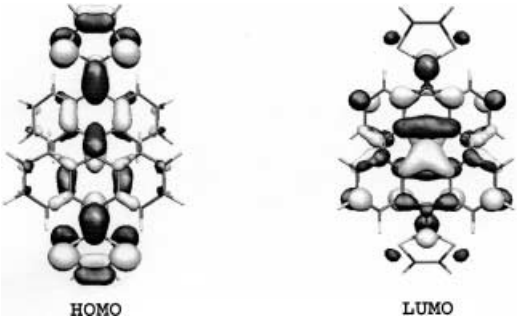

Figure 5. Electron density contours (0.03 e bohr^{-3}) calculated using the MOLDEN graphics interface for the HOMO and the LUMO of **11a**.

charge transfer. In contrast to the experimental absorption data, TDDFT calculations predict a sizeable bathochromic shift on going from **2a**, for which the HOMO→LUMO electronic transition is calculated at 3.01 eV (experimentally found 2.90 eV),[17] to **11a** (calcd 2.70 eV; found 2.87 eV).

TDDFT calculations indicate that the shoulder observed at 379 nm (3.27 eV) is due to the transition to the 2^1B_u state—calculated to lie at 3.36 eV ($f = 0.16$)—which mainly corresponds to the HOMO→LUMO+1 one-electron promotion. The absorption band at 333 nm (3.72 eV) is attributed to the transitions to the 3^1B_u and 4^1B_u states, calculated at 3.64 eV ($f = 0.14$) and 3.77 eV ($f = 0.21$), which have a high degree of multiconfigurational character (HOMO−2→LUMO, HOMO−1→LUMO+2, etc.). The calculated vertical excitation energies are in good agreement with the experimental values and permit a comprehensive assignment of the spectrum.

Oxidized compounds: The equilibrium geometries of the cation and dication of **11a** were computed at the B3P86/6-31G* level to investigate how the oxidation process affects the molecular structure and the electronic properties of the molecule. The molecular geometries calculated for **11a**$^{\bullet+}$ and **11a**$^{2+}$ were optimized under different symmetry restrictions. Figure 4b and c display the optimized bond lengths corresponding to the minimum-energy conformations calculated for **11a**$^{\bullet+}$ and **11a**$^{2+}$, respectively.

Oxidation affects the whole molecule by modifying the lengths of the bonds in which the electron density in the HOMO, that is, the orbital from which electrons are removed, is concentrated. In this way, the largest changes correspond to: i) the central C9−C9′ bond, which lengthens from 1.363 Å (**11a**) to 1.496 Å (**11a**$^{2+}$), ii) the exocyclic C10−C15 and C10′−C15′ bonds, which lengthen from 1.360 to 1.459 Å, iii) the C15−S and C15′−S bonds, which shorten from 1.778 to 1.705 Å, and iv) the bonds connecting the outer benzene rings of the anthracene units to the C9,C9′ and C10,C10′ atoms, which shorten from 1.47–1.48 to 1.41–1.42 Å. The bond lengths obtained for the cation are similar to those in the neutral molecule (cf. Figure 4a and b), because both species show the same molecular conformation.

After removal of the first electron—to generate the cation—the molecule retains the C_{2h} conformation of the neutral system (Figure 3b). The most stable conformation of **11a**$^{\bullet+}$ thus corresponds to a butterfly-shaped structure, in which the distortions from planarity are slightly reduced with respect to the neutral molecule. In particular, the folding of the anthracene units decreases from 42.3 to 39.7° and the tilt angle of the dithiole rings decreases from 34.5 to 32.3°.

In contrast, the removal of the second electron—to form the dication—leads to more marked effects on the molecular conformation. The lengthening of the exocyclic bonds allows rotation of the dithiole and anthracene units to minimize the steric interactions. The minimum-energy conformation of **11a**$^{2+}$ thus corresponds to the D_2 structure depicted in Figure 6a. In this D_2 structure, the anthracene units are almost planar and adopt a mutually orthogonal disposition, while the dithiole rings are twisted out of the anthracene planes by 63.8°. The butterfly-shaped C_{2h} structure obtained for **11a** and **11a**$^{\bullet+}$ was also considered for **11a**$^{2+}$, but it was found to be 28.90 kcal mol^{-1} higher in energy. The predicted D_2 conformation was calculated to be 0.79 kcal mol^{-1} more stable than the D_{2d} conformation, in which the four subunits constituting the molecule are fully planar and orthogonal. The conformation predicted for **11a**$^{2+}$ is similar to that obtained for **2a**$^{2+}$,[3] for which B3P86/6-31G* calculations predict a D_{2h} structure with the dithiole rings twisted by 90°, in agreement with experimental data.[4a,19]

The D_2 conformation of **11a**$^{2+}$ was used as an alternative structure in the search for the most stable conformation of **11a**$^{\bullet+}$. The calculation converged to a D_2 structure, in which the anthracene units are twisted by 78.9° about the central C9−C9′ bond and the dithiole rings are rotated by 55.7° with respect to the anthracene planes. Relative to the C_{2h} structure, the resulting structure is only 1.90 kcal mol^{-1} higher in energy. This small energy difference suggests that both structures (C_{2h} and D_2) may be involved in the formation of **11a**$^{\bullet+}$. Considering the related system, 9,9′-bianthrone, both structures have indeed been shown to play a role in the mechanism for the reduction of this molecule.[25] To investigate the possible influence of the solvent on the relative stabilities of the C_{2h} and D_2 conformations, the total energies of the optimized structures were calculated in the presence of solvents using the Polarized Continuous Model (PCM).[26] The energy difference between the two structures increases slightly to 2.49 kcal mol^{-1} in dichloromethane and to 2.77 kcal mol^{-1} in the more polar solvent dimethyl sulfoxide. These energy values indicate that, although the C_{2h} structure is more stable for **11a**$^{\bullet+}$, the formation of the D_2 structure cannot be discarded.

The bond lengths calculated for the anthracene units in the minimum-energy D_2 conformation of **11a**$^{2+}$ (Figure 4c) are almost identical to those obtained for the anthracene molecule in its neutral state (Figure 4d). This result suggests that in **11a**$^{2+}$ the electrons have been mainly removed from the dithiole rings, while the anthracene units remain essentially neutral. The net atomic charges calculated using the Natural Population Analysis (NPA) algorithm[27] confirm this assumption, since each dithiole ring in **11a**$^{2+}$ is found to bear a positive charge of +0.82 e. Therefore, we visualize the dications of compounds **11** as a central 9,9′-bianthryl unit substituted by singly-charged dithiole rings. Thus, the dications consist of four aromatic, orthogonally-oriented π-

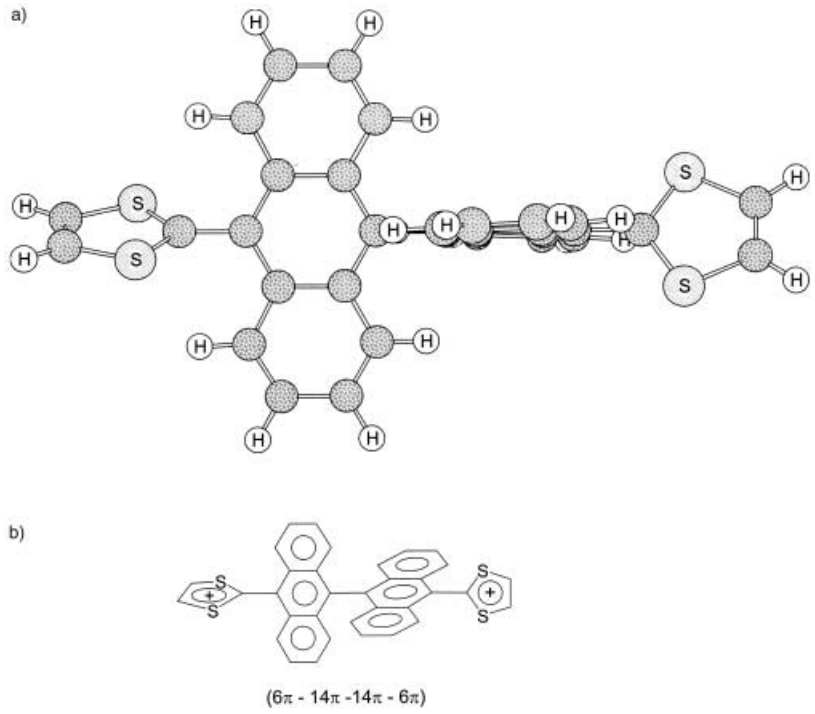

Figure 6. a) Minimum-energy B3P86/6-31G* conformation (D_2 symmetry) calculated for $\mathbf{11a}^{2+}$. b) Molecular structure of $\mathbf{11a}^{2+}$ showing the number of π-electrons of each aromatic subunit.

systems, as sketched in Figure 6b. The D_2 conformation obtained for $\mathbf{11a}^{\cdot+}$ shows a similar structure, with a positive charge of +0.44 e (+0.37 e for the C_{2h} conformation) residing on each dithiole ring and almost neutral anthracene units.

As for **2**,[3,4a,19,20] the electrochemical behavior of **11** can be rationalized in terms of the conformational changes predicted for these extended TTFs upon oxidation. The removal of the first electron would, in principle, lead to the radical cation in the most stable C_{2h} conformation, which retains the butterfly-shaped structure of the neutral molecule. As soon as the cation is formed, it is oxidized to the dication. For example, in dichloromethane, the energy required for the first ionization process **11a** (C_{2h}) → $\mathbf{11a}^{\cdot+}$ (C_{2h}) (5.42 eV) is calculated to be larger than that required for the second ionization process $\mathbf{11a}^{\cdot+}$ (C_{2h}) → $\mathbf{11a}^{2+}$ (D_2) (5.15 eV). These ionization energies are thus consistent with the coalescence of the first two oxidation processes under the same CV wave observed experimentally for **11**. The high stability of the dications $\mathbf{11}^{2+}$ can be attributed to their highly aromatic structure, being composed of four aromatic subunits. Moreover, the large distance between the dithiole rings (~12 Å) is too great for any significant coulombic repulsion between the extra charges introduced upon oxidation at these rings. The pronounced electrochemical irreversibility measured for the oxidation wave ($E_{ap}-E_{cp} > 0.9$ V) can be attributed to the large structural rearrangement that must take place upon reduction [$\mathbf{11}^{2+}(D_2)$ → $\mathbf{11}(C_{2h})$], which implies the loss of aromaticity of all four constituent units.

As indicated in the introduction, the design of compounds **11** has been pursued with a view to integrating them as electron-donor units in C_{60}-based D–A systems for photovoltaic applications. The outstanding gain of aromaticity that compounds **11** undergo on going from the neutral molecule (C_{2h}) to the oxidized species (D_2 conformations) can be envisaged as playing a primary role in stabilizing the light-induced intramolecular charge-separated state and thereby in increasing the lifetime of that state.

Pulse radiolysis: The two-electron nature of the oxidation processes that **11a–c** exhibited in the cyclic voltammetry experiments prompted us to probe their selective one-electron and two-electron oxidation by radiation chemical methods. Here, the reaction under investigation is the radiation-sensitized one-electron transfer from **11a–c** in a non-polar solvent, in this case 1,2-dichloroethane. The main products of the radiolysis of $C_2H_4Cl_2$ are i) the parent radical cations and ii) free radical species. The latter are formed by dissociative capture of the ionization electrons according to Equation (1).

$$2\,C_2H_4Cl_2 \xrightarrow{\text{radiolysis}} C_2H_4Cl_2^{\cdot+} + {}^{\cdot}C_2H_4Cl + Cl^- \quad (1)$$

Because of the short lifetime of the parent ion, about 130 ns, and to avoid interference with its fragmentation products, it was necessary to add 0.5 M benzene, which leads to quantitative conversion of the metastable parent ion into the stable benzene radical cation according to Equation (2). Under the described experimental conditions, the benzene radical cations exist in a monomer-dimer equilibrium according to Equation (3),[28] but we could nevertheless observe the electron transfer from solutes **11a–c** at the 0.1 mM level as a result of reaction according to Equation (4).

$$C_2H_4Cl_2^{\cdot+} + C_6H_6 \rightarrow C_6H_6^{\cdot+} + C_2H_4Cl_2 \quad (2)$$

$$C_6H_6^{\cdot+} + C_6H_6 \rightleftharpoons (C_6H_6)_2^{\cdot+} \quad (3)$$

$$\pi\text{-extended TTF} + C_6H_6^{\cdot+} \rightarrow (\pi\text{-extended TTF})^{\cdot+} + C_6H_6 \quad (4)$$

Based on this concept, pulse radiolysis measurements by means of optical absorption spectroscopy were performed using 10 nanosecond pulses. This enabled the direct and time-resolved monitoring of process (4). Upon radiolysis of nitrogen-purged solutions of **11a–c** (~10^{-4} M) in $C_2H_4Cl_2$ containing 0.5 M benzene, pronounced changes in absorption were noted throughout the visible part of the spectrum. This

is illustrated in Figures 7 and 8. For **11a**, a net decrease in absorption centered at around 430 nm was observed, a region in which the ground-state absorption of the parent compound predominates. Furthermore, absorptions centered at around $\lambda_{max} = 350$, 500, and 620 nm in the visible and an additional feature in the infrared region < 900 nm were detected. From i) the absorption changes and ii) the absorption–time profiles—characteristic examples are illustrated as insets in Figure 7—the existence of two different transients can be established. Firstly, we note a direct product of the electron-transfer event [Eq. (4)], which absorbs at around 620 nm. Secondly, a subsequent product, formed by second-order decay of the initial one, is seen with absorptions between 350 and 500 nm. A concentration variation, that is, varying the radiation dose, confirmed that the formation of the subsequent product strictly obeys a second-order rate law. The second-order kinetics of formation and the long lifetime of the formed species ($\tau \gg 10$ ms) led us to consider a disproportionation reaction of the metastable π-radical cation [Eq. (5)], generating the corresponding dication of **11a**.

$$2\,(\pi\text{-extended TTF})^{\cdot+} \rightarrow (\pi\text{-extended TTF})^{2+} + \pi\text{-extended TTF} \quad (5)$$

As regards the kinetics of the electron-transfer sequence [i.e., Eqs. (2) to (4)], the time profiles shown as insets in Figure 7 help to corroborate the mechanistic considerations. On a time scale of up to 2.5 μs, the decay of the benzene radical cation, which has maxima at 440 and 900 nm, is linked to the consumption of the parent **11a** (i.e., depletion at 430 nm). Due to significant spectral superposition, the formation of (π-extended TTF)$^{\cdot+}$ at 620 nm is partly masked, but an evident trend is nevertheless discernible in the 500 and 620 nm profiles, especially on the longer time scales. These profiles also show the kinetics of reaction according to Equation (5), that

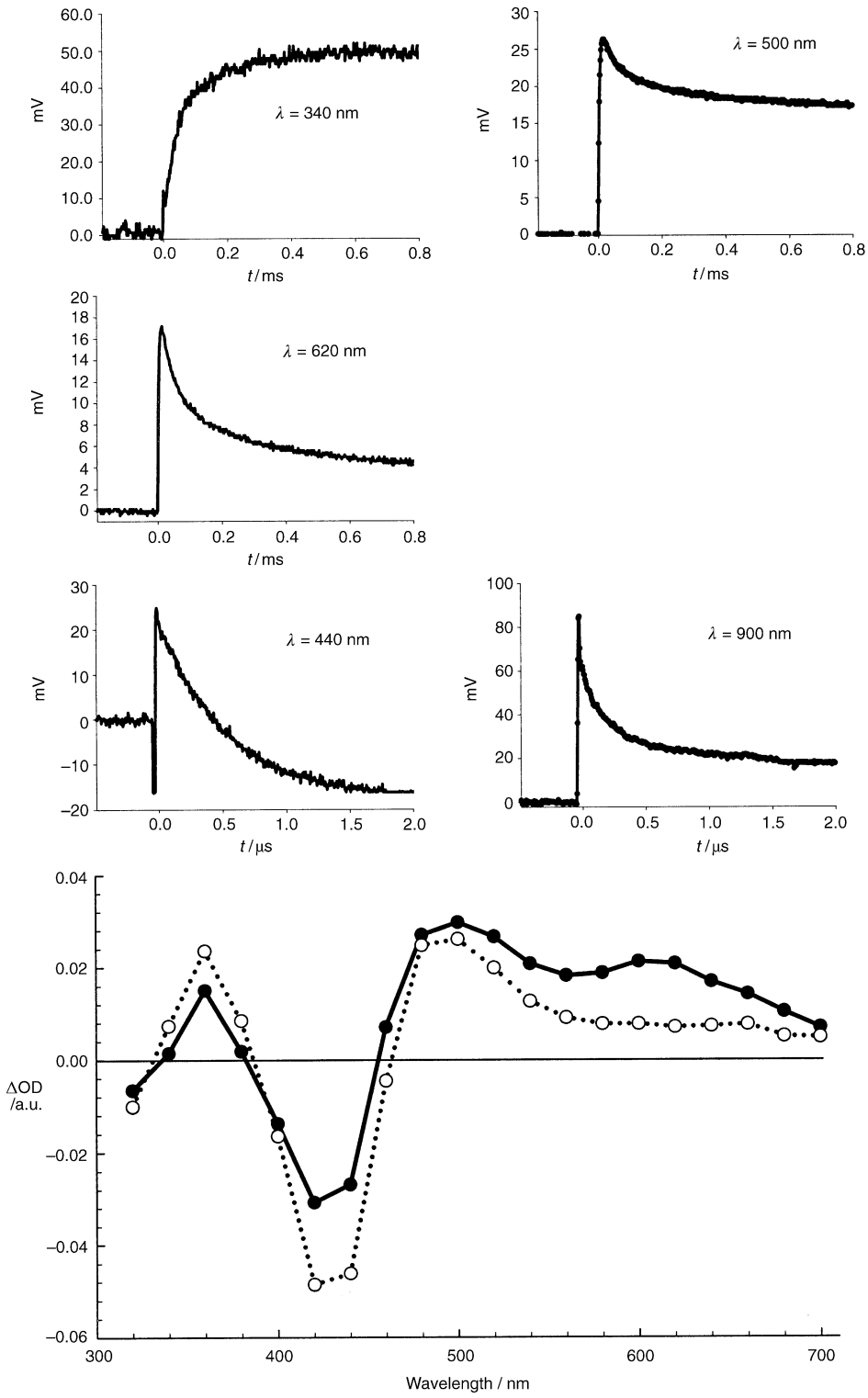

Figure 7. Differential absorption spectrum (UV/Vis spectrum) and time profiles taken in the pulse radiolytic oxidation of **11a** (0.1 mM) in nitrogen-purged 1,2-dichloroethane containing 0.5 M benzene. The spectra were taken immediately after the electron pulse (●) and after 600 μs (○). The time profiles were taken at the indicated wavelengths.

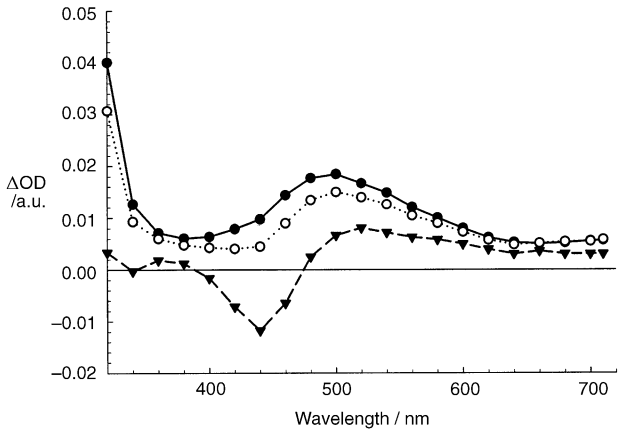

Figure 8. Differential absorption spectrum (UV/Vis spectrum) and time profiles taken in the pulse radiolytic oxidation of **11c** (0.1 mM) in nitrogen-purged 1,2-dichloroethane containing 0.5 M benzene; (●), (○), (▽).

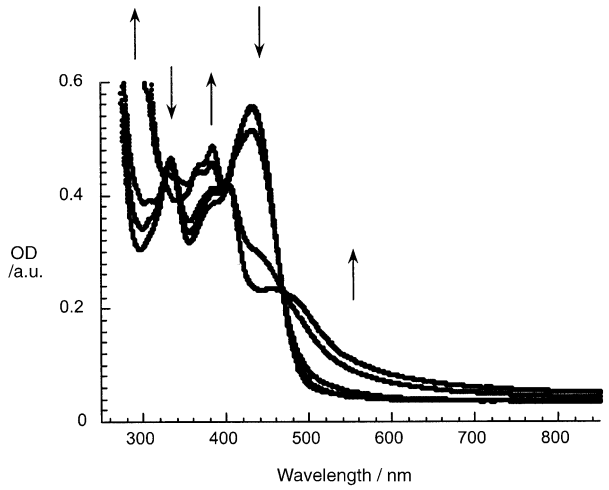

Figure 9. Radiolytic oxidation of **11a** in oxygenated dichloroethane solutions. γ-Radiolytic oxidation; the doses were 0, 50, 100, 200, 400, and 600 Gy; the arrows indicate the direction of absorption changes during the course of irradiation.

is, the decay of absorption at 620 nm due to (π-extended TTF)$^{\bullet+}$ and the presence of that at 500 nm due to (π-extended TTF)$^{2+}$ as the long-term stable product. The 340 nm profile shows the formation of (π-extended TTF)$^{2+}$ most clearly.

It should be emphasized that oxygen exerts no significant influence on the reactivity, whereas ethanol serves as a good cation quencher. Analogous data were recorded for compounds **11b**,**c**, with only slight differences in their absorption features. This is illustrated by Figure 8, which shows the transient absorption behavior recorded for **11c**.

The absorption minima (corresponding to bleaching of the ground state) and maxima (corresponding to new transient absorptions) of the π-radical cations of **11a–c** are collected in Table 1. Here, it must be pointed out that additional broad features are seen in the near-infrared region—as illustrated in the case of **11c**—the absolute maxima of which could not be determined with precision.

Table 1. Absorption maxima (λ_{max} in nm) of neutral, radical cation, and dication species of **11a–c**.

Compound	Neutral	Radical cation	Dication
11a	430	490, 620	383, 452
11b	435	550, 650	372, 418
11c	440	510, 600 (sh)	372, 414

To examine furthermore i) the stabilities of the π-radical cations and ii) the second one-electron oxidation step yielding the corresponding dications of **11a–c**, complementary steady-state γ-radiolyses were conducted. In particular, the optical absorption spectra of π-extended TTFs **11a–c** in oxygenated $C_2H_4Cl_2$ were recorded before and after various periods of irradiation; see Figure 9. The peaks of the starting material, for example those of **11a** at 330 and 430 nm, gradually decayed upon irradiation while new peaks arose, in this case at 383 and 452 nm. An additional feature is seen in the 650–800 nm region, but the weak absorbances and poor spectral resolution preclude an exact determination of the peak maximum. In general, these spectral features are markedly blue-shifted with respect to those observed at short times after the electron pulse (140 μs). Specifically, no indication of the characteristic fingerprint of the π-radical cation was found in the region between 500 and 620 nm.

In steady-state radiolysis, the newly formed species is stable and no subsequent change in absolute absorption was detected over several hours following the initial irradiation. The good isosbestic points (at 397 and 470 nm) unequivocally indicate a clean radiolytic transformation of the starting ground state into the stable product. γ-Radiolysis of similar solutions of π-extended TTFs **11b** and **11c** also resulted in a gradual disappearance of the 435 and 440 nm peaks, while new peaks developed at 418 and 414 nm, respectively (see Table 1). All these experimental observations are consistent with the hypothesis of a stepwise two-electron oxidation of **11a–c**, via the transient, short-lived (π-extended TTF)$^{\bullet+}$ π-radical cation, to the corresponding (π-extended TTF)$^{2+}$ dication.

On closer inspection of Table 1, the minima of the bleaching parts in the transient absorption spectra reveal an interesting trend. Successive and gradual red shifts, which nicely mirror the corresponding ground-state maxima, are seen upon varying the substitution pattern of the TTF rings, for example, from R = H (430 nm) (**11a**), to R = SCH_3 (435 nm) (**11b**), to R = -SCH_2CH_2S- (440 nm) (**11c**).

In **11a**$^{2+}$, the π-orbitals are quasi-degenerate in a pairwise manner due to the near-orthogonality of the constituent subunits. The HOMO of **11a**$^{2+}$ extends over the anthracene units and its AO composition corresponds to that of the HOMO of anthracene. In contrast, the LUMO is located on the dithiole rings, which, in the case of **11a**$^{2+}$, are electron deficient. The TDDFT approach predicts that the first electronic excited state of **11a**$^{2+}$, calculated to lie at 1.59 eV (781 nm, $f = 0.15$), should result from the HOMO→LUMO one-electron excitation. Thus, we assign the weak absorptions observed in the 650–800 nm region to an intramolecular charge transfer from the anthracene units to the outer di-

thiole rings. The low intensity observed experimentally for this absorption can be attributed to the more perpendicular disposition adopted by the dithiole rings of $\mathbf{11a}^{2+}$ in solution, which renders the charge transfer more difficult. In fact, the HOMO→LUMO transition has zero oscillator strength for the fully orthogonal D_{2d} conformation.

The absorption band observed at 452 nm (2.74 eV) is assigned to the electronic transition calculated at 2.98 eV (f = 0.24). The MOs involved in the transition reside on the anthracene moieties and their AO compositions reveal that this band actually corresponds to the HOMO→LUMO transition of neutral anthracene. The energy calculated for the transition is intermediate between those obtained for $\mathbf{2a}^{2+}$ (2.84 eV) and anthracene (3.28 eV) at the same computational level. This trend is borne out by the experimental values ($\mathbf{2a}^{2+}$: 2.65 eV;[17] $\mathbf{11a}^{2+}$: 2.74 eV; anthracene: 3.31 eV)[29] and reflects the effect of the extra charge on the optical properties of the anthracene moieties.

Conclusion

In summary, we have described a new series of highly conjugated π-extended TTF derivatives (**11a–c**) obtained by Wittig–Horner reaction from commercially available bianthrone and phosphonate esters **10a–c**. DFT theoretical calculations (B3P86/6-31G*) predict a highly distorted neutral molecule for **11a**, in which the HOMO is localized on the 1,3-dithiole rings and the LUMO extends over the anthracene moiety. Thus, the HOMO→LUMO transition corresponds to the low-energy charge-transfer absorption band (~430 nm) observed in the UV/Vis spectrum of the neutral molecule **11a**.

The HOMO energy (**11a**: −5.35 eV) is consistent with cyclic voltammetry measurements, which reveal that these compounds exhibit good donor properties showing a two-electron oxidation wave to form the dication species. The oxidation process has been studied by optimizing the molecular structures of the monocations and dications. Theoretical calculations predict that the gain of aromaticity is small for the monocations, since they remain highly distorted from planarity and retain the geometry of the neutral molecule. On the contrary, the dications are fully aromatic with four orthogonally oriented π-systems. The lower stability of the monocation and the high aromaticity of the dication account for the coalescence of the first two oxidation potentials within the same oxidation wave.

Pulse radiolysis measurements support the above conclusions, showing that the intermediate radical cation species can be characterized, but quickly disproportionates to form the more stable dication species.

The remarkable gain of aromaticity of compounds **11a–c** on going from the neutral to the dication state suggests that these donor molecules might be of interest as building blocks in the construction of novel D–A dyads with charge-separated states exhibiting outstanding lifetimes.

Experimental Section

Computational details: All theoretical calculations were carried out at the DFT level using the A.11 revision of the Gaussian 98 program package[30] running on IBM RS/6000 workstations at the Instituto de Ciencia Molecular of the University of Valencia. The DFT calculations were performed using Becke's three-parameter B3P86 exchange-correlation functional[31] together with the 6-31G* basis set.[32] The B3P86 functional has been recognized as providing equilibrium geometries for sulfur-containing compounds in better accord with experimental data and ab initio post-Hartree–Fock (HF) calculations than the more widely used B3LYP functional.[33] The radical cations were treated as open-shell systems and were computed using spin-unrestricted UB3P86 wavefunctions. Vertical electronic excitation energies were obtained by means of the TDDFT approach.[34] Numerous hitherto reported applications indicate that TDDFT employing current exchange-correlation functionals performs significantly better than HF-based single-excitation theories for the low-lying valence excited states.[20,35] TDDFT calculations were also performed using the B3P86 functional and the 6-31G* basis set.[36]

Radiation chemistry: Steady-state irradiations were carried out in a Gammacell 220 with a ^{60}Co source at a dose rate of 9 Gy s^{-1}. Irradiation times were up to several minutes. Optical absorption spectra were recorded before and several minutes after irradiation. Pulse radiolysis experiments were performed using 10 ns pulses of 1 MeV electrons from an ELIT transformer-type electron accelerator (Institute of Nuclear Physics, Novosibirsk, Russia). Details of the equipment and the data acquisition have been described elsewhere.[37] Dosimetry was based on optical observation of the solvated electron (after 100 ns) in slightly alkaline solution calibrated with G ≈ 2.6 (G denotes the number of species per 100 eV, or the approximate μM concentration per 10 J of absorbed energy). The radical concentration generated per pulse varied in the range (1–3) × 10^{-5} M.

Compounds 11a–c: *n*-Butyllithium (BuLi) (1.6 M in hexane; 1.1 mmol) was added to a stirred solution of the corresponding Wittig–Horner reagent **10a–c** (1 mmol) in dry THF (50 mL) at −78 °C under argon atmosphere by means of a syringe. After 30 minutes at −78 °C, a solution of the bianthrone **9** (96 mg, 0.25 mmol) in dry THF (10 mL) was added to the solution of the generated phosphonate carbanion, also by means of a syringe. The mixture was stirred for 1 h at −78 °C and then allowed to warm to 20 °C overnight. The products were purified by column chromatography on silica gel, eluting with cyclohexane/toluene (1:1), to afford compounds **11a–c** as stable orange solids.

10,10′-Bis(1,3-dithiol-2-ylidene)-9,9′-bis(9,10-dihydroanthracene) (11a): Yield 51%; m.p. > 250 °C; ^{1}H NMR (300 MHz, $CDCl_3$): δ = 7.70–7.67 (m, 4H), 7.23–7.19 (m, 4H), 7.09–7.05 (m, 4H), 7.00–6.92 (m, 4H), 6.34 (s, 4H); EI-MS: m/z: 556 [M^+]; IR (KBr): $\tilde{\nu}_{max}$ = 1570, 1545, 1518, 1261, 941, 752, 657 cm^{-1}; UV/Vis (CH_2Cl_2): λ_{max} = 431, 378 (s), 333, 236 nm.

10,10′-Bis(4,5-dimethylthio-1,3-dithiol-2-ylidene)-9,9′-bis(9,10-dihydroanthracene) (11b): Yield 64%; m.p. > 250 °C; ^{1}H NMR (300 MHz, $CDCl_3$): δ = 7.69–7.65 (m, 4H), 7.22–7.18 (m, 4H), 7.08–7.04 (m, 4H), 6.99–6.95 (m, 4H), 2.50 (s, 12H); EI-MS: m/z: 740 [M^+]; IR (KBr): $\tilde{\nu}_{max}$ = 2947, 1535, 1499, 1446, 1227, 1055, 825, 750, 639 cm^{-1}; UV/Vis (CH_2Cl_2): λ_{max} = 436, 376 (s), 337, 241 nm.

10,10′-Bis(4,5-diethylenedithio-1,3-dithiol-2-ylidene)-9,9′-bis(9,10-dihydroanthracene) (11c): Yield 71%; m.p. > 250 °C; ^{1}H NMR (300 MHz, $CDCl_3$): δ = 7.64–7.60 (m, 4H), 7.20–7.17 (m, 4H), 7.09–7.06 (m, 4H), 7.00–6.92 (m, 4H), 3.37 (m, 8H); EI-MS: m/z: 737 [M^+]; IR (KBr): $\tilde{\nu}_{max}$ = 2920, 1521, 1446, 1413, 1284, 750, 638 cm^{-1}; UV/Vis (CH_2Cl_2): λ_{max} = 450, 342, 241 nm.

Acknowledgements

Financial support from the MCYT of Spain (Projects BQU2002-00855, BQU2002-10656-E, and BQU2003-05111) and from the Deutsche Forschungsgemeinschaft is greatly acknowledged. Part of this work was supported by the Office of Basic Energy Sciences of the US Department of Energy (Contribution No. NDRL4512 from the Notre Dame Radiation Laboratory). I.Z. acknowledges his sabbatical leave from the Nuclear Research Centre, Beer Sheva, Israel.

[1] *Handbook of Organic Conductive Molecules and Polymers, Vol. 1* (Ed.: H. S. Nalwa), Wiley, Chichester, **1997**.

[2] For recent reviews on TTF, see: a) J. L. Segura, N. Martín, *Angew. Chem.* **2001**, *113*, 1416–1455; *Angew. Chem. Int. Ed.* **2001**, *40*, 1372–1409; b) M. R. Bryce, *J. Mater. Chem.* **2000**, *10*, 589–598; c) M. B. Nielsen, C. Lomholt, J. Becher, *Chem. Soc. Rev.* **2000**, *29*, 153–164.

[3] N. Martín, L. Sánchez, C. Seoane, E. Ortí, P. M. Viruela, R. Viruela, *J. Org. Chem.* **1998**, *63*, 1268–1279.

[4] a) M. R. Bryce, A. J. Moore, M. Hasan, G. J. Ashwell, A. T. Fraser, W. Clegg, M. B. Hursthouse, A. I. Karaulov, *Angew. Chem.* **1990**, *102*, 1493–1495; *Angew. Chem. Int. Ed. Engl.* **1990**, *29*, 1450–1452; b) Y. Yamashita, Y. Kobayashi, T. Miyashi, *Angew. Chem.* **1989**, *101*, 1090–1091; *Angew. Chem. Int. Ed. Engl.* **1989**, *28*, 1052–1053.

[5] a) M. A. Herranz, N. Martín, L. Sánchez, J. Garín, J. Orduna, R. Alcalá, B. Villacampa, C. Sánchez, *Tetrahedron* **1998**, *54*, 11651–11658; b) M. Otero, M. A. Herranz, C. Seoane, N. Martín, J. Garín, J. Orduna, R. Alcalá, B. Villacampa, *Tetrahedron* **2002**, *58*, 7463–7475. See also: M. González, J. L. Segura, C. Seoane, N. Martín, J. Garín, J. Orduna, R. Alcalá, B. Villacampa, V. Hernández, J. T. López Navarrete, *J. Org. Chem.* **2001**, *66*, 8872–8882.

[6] M. R. Bryce, A. S. Batsanov, T. Finn, T. K. Hansen, J. A. K. Howard, M. Kamenjicki, I. K. Lednev, S. A. Asher, *Chem. Commun.* **2000**, 295–296.

[7] D. F. Perepichka, M. R. Bryce, I. F. Perepichka, S. B. Lyubchik, Ch. A. Christensen, N. Godbert, A. Batsanov, E. Levillain, E. J. L. McInnes, J. P. Zhao, *J. Am. Chem. Soc.* **2002**, *124*, 14227–14238.

[8] a) M. A. Herranz, N. Martín, *Org. Lett.* **1999**, *1*, 2005–2007; b) Ch. A. Christensen, M. R. Bryce, A. S. Batsanov, J. A. K. Howard, J. O. Jeppesen, J. Becher, *Chem. Commun.* **1999**, 2433–2434; c) M. R. Bryce, T. Finn, A. J. Moore, *Tetrahedron Lett.* **1999**, *40*, 3271–3274; d) M. R. Bryce, T. Finn, A. J. Moore, A. S. Batsanov, J. A. K. Howard, *Eur. J. Org. Chem.* **2000**, 51–60; e) N. Godbert, M. R. Bryce, S. Dahaoui, A. S. Batsanov, J. A. K. Howard, P. Hazendonk, *Eur. J. Org. Chem.* **2001**, 749–757; f) M. C. Díaz, B. M. Illescas, N. Martín, *Tetrahedron Lett.* **2003**, *44*, 945–948.

[9] a) N. Martín, I. Pérez, L. Sánchez, C. Seoane, *J. Org. Chem.* **1997**, *62*, 5690–5695; b) N. Martín, L. Sánchez, D. M. Guldi, *Chem. Commun.* **2000**, 113–114; c) M. A. Herranz, N. Martín, L. Sánchez, C. Seoane, D. M. Guldi, *J. Organomet. Chem.* **2000**, *599*, 2–7; d) M. A. Herranz, N. Martín, J. Ramey, D. M. Guldi, *Chem. Commun.* **2002**, 2968–2969; e) S. González, N. Martín, A. Swartz, D. M. Guldi, *Org. Lett.* **2003**, *5*, 557–560; f) M. C. Díaz, M. A. Herranz, B. M. Illescas, N. Martin, N. Godbert, M. R. Bryce, Ch. Luo, A. Swartz, G. Anderson, D. M. Guldi, *J. Org. Chem.* **2003**, *68*, 7711–7721.

[10] a) M. A. Herranz, B. M. Illescas, N. Martín, Ch. Luo, D. M. Guldi, *J. Org. Chem.* **2000**, *65*, 5728–5738; b) S. González, N. Martín, D. M. Guldi, *J. Org. Chem.* **2003**, *68*, 779–791; c) L. Sánchez, I. Pérez, N. Martín, D. M. Guldi, *Chem. Eur. J.* **2003**, *9*, 2457–2468.

[11] L. Echegoyen, L. E. Echegoyen, *Acc. Chem. Res.* **1998**, *31*, 593–601.

[12] a) N. Martín, L. Sánchez, B. M. Illescas, I. Pérez, *Chem. Rev.* **1998**, *98*, 2527–2548; b) *Fullerenes: From Synthesis to Optoelectronic Properties* (Eds.: D. M. Guldi, N. Martín), Kluwer, Dordrecht, The Netherlands, **2002**.

[13] N. Martín, E. Ortí, *Handbook of Advanced Electronic and Photonic Materials and Devices, Vol. 3* (Ed.: H. S. Nalwa), Academic Press, San Diego, **2001**, pp. 245.

[14] a) D. M. Guldi, *Chem. Commun.* **2000**, 321; b) D. M. Guldi, *Chem. Soc. Rev.* **2002**, *31*, 22–36.

[15] The synthesis of **11a** has been previously reported. See: A. J. Moore, M. R. Bryce, *J. Chem. Soc. Perkin Trans. 1* **1991**, 157. For other related bianthrone derivatives, see: M. Jorgensen, K. Lerstrup, P. Frederiksen, T. Bjornholm, P. Sommer-Larsen, K. Schaumburg, K. Brunfeldt, K. Bechgaard, *J. Org. Chem.* **1993**, *58*, 2785–2790.

[16] A. J. Moore, M. R. Bryce, *Synthesis* **1991**, 26–28.

[17] D. M. Guldi, L. Sánchez, N. Martín, *J. Phys. Chem. B* **2001**, *105*, 7139–7144.

[18] a) C. Wartelle, R. Viruela, P. M. Viruela, F. X. Sauvage, M. Sallé, E. Ortí, E. Levillain, F. Le Derf, *Phys. Chem. Chem. Phys.* **2003**, *5*, 4672–4679; J. Orduna, J. Garín, unpublished results.

[19] a) S. Triki, L. Ouahab, D. Lorcy, A. Robert, *Acta Crystallogr.* **1993**, *C49*, 1189–1192; b) M. R. Bryce, T. Finn, A. S. Batsanov, R. Kataky, J. A. K. Howard, S. B. Lyubchik, *Eur. J. Org. Chem.* **2000**, 1199–1205; c) A. E. Jones, C. A. Christensen, D. F. Perpichka, A. S. Batsanov, A. Beeby, P. J. Low, M. R. Bryce, A. W. Parker, *Chem. Eur. J.* **2001**, *7*, 973–978; d) C. A. Christensen, A. S. Batsanov, M. R. Bryce, J. A. K. Howard, *J. Org. Chem.* **2001**, *66*, 3313–3320.

[20] a) M. R. Bryce, M. A. Coffin, M. B. Hursthouse, A. I. Karaulov, K. Müllen, H. Scheich, *Tetrahedron Lett.* **1991**, *32*, 6029–6032; b) I. Pérez, S.-G. Liu, N. Martín, L. Echegoyen, *J. Org. Chem.* **2000**, *65*, 3796–3803; c) S.-G. Liu, I. Pérez, N. Martín, L. Echegoyen, *J. Org. Chem.* **2000**, *65*, 9092–9102.

[21] N. Martín, E. Ortí, L. Sánchez, P. M. Viruela, R. Viruela, *Eur. J. Org. Chem.* **1999**, 1239–1247.

[22] W. Koch, M. C. Holthausen, *A Chemist's Guide to Density Functional Theory*, Wiley-VCH, Weinheim, Germany, **2000**.

[23] E. Harnik, G. M. J. Schmidt, *J. Chem. Soc.* **1954**, 3295–3302.

[24] S. Yamaguchi, T. Hanafusa, T. Tanaka, M. Sawada, K. Kondo, M. Irie, H. Tatemitsu, Y. Sakata, S. Misumi, *Tetrahedron Lett.* **1986**, *27*, 2411–2414.

[25] a) B. A. Olsen, D. H. Evans, *J. Am. Chem. Soc.* **1981**, *103*, 839–843; b) P. Neta, D. H. Evans, *J. Am. Chem. Soc.* **1981**, *103*, 7041–7045; c) S. M. Mattar, D. G. Sutherland, *J. Phys. Chem.* **1991**, *95*, 5129–5133.

[26] In the PCM approach, the solvent is considered as a continuous medium with a dielectric constant ε, and the solute is represented by means of a cavity built-up from a number of interlaced atomic spheres. a) M. Cossi, V. Barone, R. Cammi, J. Tomasi, *Chem. Phys. Lett.* **1996**, *255*, 327–335; b) C. Amovilli, V. Barone, R. Cammi, E. Cancès, M. Cossi, B. Menucci, C. S. Pomelli, J. Tomasi, *Adv. Quantum Chem.* **1999**, *32*, 227–261.

[27] A. E. Reed, L. A. Curtiss, F. Weinhold, *Chem. Rev.* **1988**, *88*, 899–926.

[28] T. Shida, *Electronic Absorption Spectra of Radical Ions*, Elsevier, Amsterdam, **1988**, pp. 12.

[29] H. H. Perkampus, *UV-Vis Atlas of Organic Compounds*, VCH, Weinheim, **1992**.

[30] *Gaussian 98*, Revision A.11, M. J. Frisch, G. W. Trucks, H. B. Schlegel, G. E. Scuseria, M. A. Robb, J. R. Cheeseman, V. G. Zakrzewski, J. A. Montgomery, R. E. Stratman, J. C. Burant, S. Dapprich, J. M. Millam, A. D. Daniels, K. N. Kudin, M. C. Strain, O. Farkas, J. Tomasi, V. Barone, M. Cossi, R. Cammi, B. Mennucci, C. Pomelli, C. Adamo, S. Clifford, J. Ochterski, G. A. Petersson, P. Y. Ayala, Q. Cui, K. Morokuma, P. Salvador, J. J. Danenberg, D. K. Malick, A. D. Rabuck, K. Raghavachari, J. B. Foresman, J. Cioslowski, J. V. Ortiz, A. G. Baboul, B. B. Stefanov, G. Liu, A. Liashenko, P. Piskorz, I. Komaromi, R. Gomperts, R. L. Martin, D. J. Fox, T. Keith, M. A. Al-Laham, C. Y. Peng, A. Nanayakkara, M. Challacombe, P. M. W. Gill, B. Johnson, W. Chen, M. W. Wong, J. L. Andres, C. Gonzalez, M. Head-Gordon, E. S. Replogle, J. A. Pople, Gaussian, Inc., Pittsburgh PA, **2001**.

[31] J. P. Perdew, *Phys. Rev. B* **1986**, *33*, 8822–8824.

[32] P. C. Hariharan, J. A. Pople, *Chem. Phys. Lett.* **1972**, *16*, 217–219.

[33] a) P. M. Viruela, R. Viruela, E. Ortí, J.-L. Brédas, *J. Am. Chem. Soc.* **1997**, *119*, 1360–1369; b) R. Liu, X. Zhou, H. Kasmai, *Spectrochim. Acta* **1997**, *53*, 1241–1256; c) J. A. Altmann, N. C. Handy, V. E. Ingamells, *Mol. Phys.* **1997**, *92*, 339–352.

[34] a) E. Runge, E. K. U. Gross, *Phys. Rev. Lett.* **1984**, *52*, 997–1000; b) E. K. U. Gross, W. Kohn, *Adv. Quantum Chem.* **1990**, *21*, 255; c) E. K. U. Gross, C. A. Ullrich, U. J. Gossmann, *Density Functional Theory* (Eds.: E. K. U. Gross, R. M. Driezler), Plenum Press, New York, **1995**, pp. 149; d) M. E. Casida, *Recent Advances in Density Functional Methods, Part I* (Ed.: D. P. Chong), World Scientific, Singapore, **1995**, pp. 155.

[35] J. Fabian, *Theor. Chem. Acc.* **2001**, *106*, 199–217.

[36] M. M. Francl, W. J. Pietro, W. J. Hehre, J. S. Binkley, M. S. Gordon, D. J. Defrees, J. A. Pople, *J. Chem. Phys.* **1982**, *77*, 3654–3665.

[37] O. Brede, H. Orthner, V. Zubarev, R. Hermann, *J. Phys. Chem.* **1996**, *100*, 7097–7105.

Received: September 19, 2003 [F5555]

